Fast Tunable High-Q-Factor Superconducting Microwave Resonators

N.B. When citing this work, cite the original published paper.

(article starts on next page)

Fast Tunable High-*Q*-Factor Superconducting Microwave Resonators

Sumedh Mahashabde,[1] Ernst Otto⬤,[1] Domenico Montemurro⬤,[1] Sebastian de Graaf,[2]
Sergey Kubatkin,[1] and Andrey Danilov[1,*]

[1] *Department of Microtechnology and Nanoscience MC2, Chalmers University of Technology,
SE-41296 Goteborg, Sweden*

[2] *National Physical Laboratory, Hampton Road, Teddington TW11 0LW, United Kingdom*

We present fast tunable superconducting microwave resonators fabricated from planar NbN on a sapphire substrate. The $3\lambda/4$ wavelength resonators are tuning fork shaped and tuned by passing a dc current that controls the kinetic inductance of the tuning fork prongs. The $\lambda/4$ section from the open end operates as an integrated impedance converter that creates a nearly perfect short for microwave currents at the dc terminal coupling points, thus preventing microwave energy leakage through the dc lines. We measure an internal quality factor $Q_{int} > 10^5$ over the entire tuning range. We demonstrate a tuning range of greater than 3% and tuning response times as short as 20 ns for the maximum achievable detuning. Because of the quasifractal design, the resonators are resilient to magnetic fields of up to 0.5 T.

I. INTRODUCTION

Superconducting microwave resonators are versatile devices with applications ranging from signal conditioning in Purcell filters [1] and parametric amplifiers [2,3] to sensing applications such as kinetic inductance detectors [4] and near field scanning microwave microscopes [5–7]. In particular, in the rapidly developing field of quantum computing superconducting resonators are used for qubit readout, on-demand storage and release [8], and routing of single microwave photons [9,10], and deployed as qubit communication buses [11]. Furthermore, future progress in quantum computing calls for identification and elimination of material defects, which spoil coherence in quantum circuits [12,13]. This urgent need stimulated the development of planar electron spin resonance (ESR) spectrometers with subfemtomole sensitivity [14,15] to environmental spins. The frequency tuning functionality either greatly benefits (filters, sensors, spectrometers) or is instrumental for (parametric amplifiers, single-photon sources) all the above applications.

The base frequency of any microwave resonator is defined by its geometry and can therefore be adjusted by varying the geometrical parameters. In practice, purely mechanical designs are bulky, challenging to implement [16], and do not provide fast tuning.

---

*andrey.danilov@chalmers.se

Conveniently, superconducting design elements provide an alternative option: any superconductor possesses kinetic inductance (KI), which can be tuned with either an external magnetic field or a dc bias current. The first approach does not require any tweaks to a standard coplanar resonator design and was presented a decade ago by Healey *et al.* [17]. However, sweeping the external magnetic field is also a rather slow solution; the kinetic inductance itself can respond in subnanosecond time (the instantaneous KI response is, for example, exploited in traveling-wave parametric amplifiers [18,19] and comb generators [20]).

A standard way to achieve fast frequency control via KI tuning is by integrating a pair of Josephson junction elements in the form of a superconducting quantum interference device (SQUID) loop in the resonator design. The highly nonlinear loop inductance can be controlled with a magnetic flux generated by a dedicated current control line, such that no external field is needed. Devices of this type achieve tuning speeds faster than the photon lifetime Q/f_0 [21], and recently a frequency tuning time less than approximately 1 ns was demonstrated [22]. Today, SQUID-tunable resonators have become a common element in circuit QED experiments [23–25]. Unfortunately, the insertion of Josephson elements degrades the resonance quality: first designs demonstrated $Q \sim 3000$, and in best-ever devices Q still does not exceed 35 000 [26]. This is significantly lower than standard nontunable coplanar resonators, where $Q \sim 10^6$ is now typical [27].

As an alternative to SQUIDs as lumped KI elements, one can exploit the kinetic inductance of the superconducting film itself. This approach does not introduce the extra internal dissipation associated with SQUIDs, but generally does increase radiation losses: the microwave energy

leaks from the cavity through the dc terminals. An obvious way to minimize the losses is to couple the dc leads at the nodes of the microwave voltage, but, due to fabrication tolerances, one does not reach $Q > 1000$ in a practical device. The leakage can be further suppressed by supplying the bias current through low-pass filters. The simplest of such filters, capacitors, provide a shunt to ground for microwaves, and thus effectively decoupling dc lines. With this design, internal quality factors up to 10^4 in tunable coplanar resonators were demonstrated in Ref. [28]. The maximum Q is limited by two factors: the filter capacitor cannot be made larger than a few tens of picofarads because of self-resonances, and the capacitor is nonideal because of the finite loss tangent of the dielectric layer. The dielectric losses were the limiting factor in Ref. [28]. With a better dielectric, such as aluminium oxide deposited by atomic layer deposition, Q factors up to 10^4 in tunable microstrip resonators have been reached [29]. Another simple filter type, an inductive-resistive filter, was reported in Ref. [30]. With the choke inductance $L_F = 2$ nH and resistance $R_F = 0.04\ \Omega$, Q factors up to 10^5 were reported. However, this solution involves the trade-off between the quality factor and the maximum tuning rate: the Q_{int} is limited by the losses in the dissipative R_F, and therefore R_F has to be kept small, and a high L_F is needed to effectively isolate R_F; both requirements slow down the response time $\tau = L_F/R_F = 50$ ns. If few-nanosecond tuning time is required, the achievable Q factor would not exceed that of SQUID-tunable resonators.

An interesting engineering solution was reported in Ref. [31]: a photonic bandgap resonator with Bragg mirrors on either side of the cavity. The mirrors were implemented as periodic stepped-impedance waveguides with a galvanically continuous center line. Such a design allows injection of a dc bias current through the center line of the excitation coplanar line. However, in practice, the insulation provided by Bragg mirrors is limited by fabrication tolerances that compromise the array periodicity and, as a consequence, the reported Q factor was only moderate (3000).

Here, we present a resonator design that incorporates an impedance converter as an integral part of the resonator circuit. The converter provides a nearly perfect short circuit for microwave currents at the dc terminal insertion points, thus preventing an energy leakage into terminals. By design, this solution imposes no limits on the frequency tuning rate and we report dissipative Q factors above one million at high photon populations and up to 2×10^5 at the single-photon level, approaching that of standard nontunable superconducting coplanar resonators.

II. METHODS

The resonator design is sketched in Figs. 1(a) and 1(b). Conceptually, the resonator core is an electromagnetic analog of the mechanical tuning fork. The coupling to a
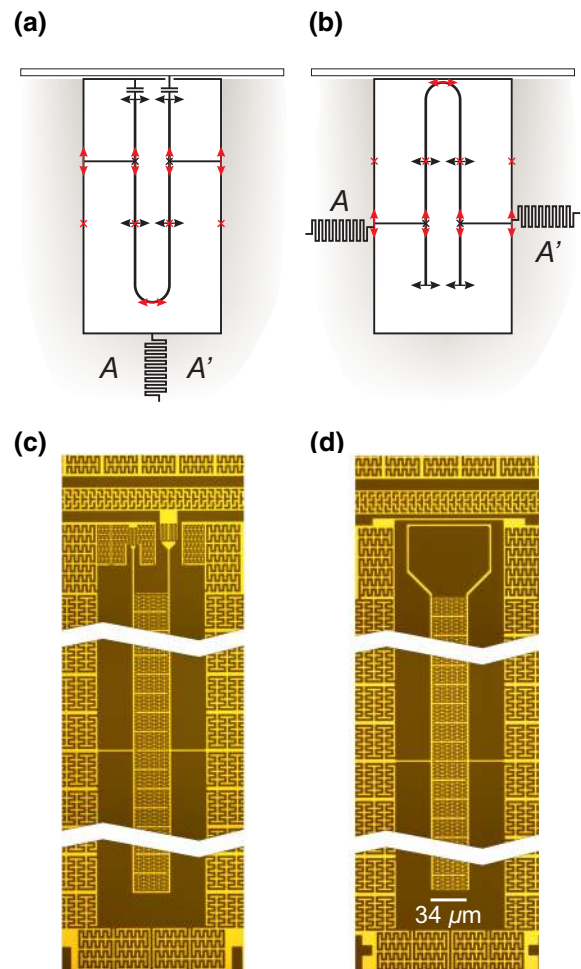

FIG. 1. Design concept and optical images. Panels (a) and (b) show cartoon representations of capacitively and inductively coupled tuning fork resonator designs. Black and red arrows show the positions of voltage and current maximums, respectively. Black and red crosses mark the positions of voltage and current nodes. We denote by A and A' two galvanically split ground half-planes. Corresponding optical images of the resonators are shown in (c) and (d).

readout coplanar waveguide transmission line is provided either via an interdigitated capacitor (a) or by an inductive loop (b). As we demonstrate below, the resulting device performance does not depend on the coupling scheme, so any solution can be freely chosen for a specific target application. The detailed design can be seen in the optical images presented in Figs. 1(c) and 1(d): the two tuning fork prongs are designed to be 2 μm in width. The prongs are inductive elements that are coupled via an interdigitated capacitor formed by a third-order quasifractal pattern. The role of the quasifractal design is discussed in detail below; in summary, it is a descendent of nontunable resonators presented earlier in Refs. [32] and [33].

We exploit the $3\lambda/4$ mode of the tuning fork. The current (voltage) nodes (antinodes) of this mode are depicted in Figs. 1(a) and 1(b): the $3\lambda/4$ mode supports a voltage

node at a distance of $\lambda/4$ from the open end of the resonator. This is the point on the prongs where we inject a dc current via a galvanic connection to the ground plane. The bias current thus flows along the closed U-turn section of the fork and controls the kinetic inductance of the resonator's $\lambda/2$ section, allowing the resonance frequency to be tuned. To allow for the dc bias, the ground plane is split into two sections, A and A', galvanically separated by one (a) or two (b) large interdigitated capacitors [sketched as meanders lines in Figs. 1(a) and 1(b)] that present negligible impedance for microwave currents (cf. Ref. [33] for further details). The finite fabrication tolerances result in some residual voltage at the nominal nodal points; the dc terminal lines, if present, couple to this voltage as antennas, resulting in radiation losses. On the contrary, the split ground plane solution eliminates radiating dc lines; the residual currents instead circulate across the splitting capacitor. Most crucially, the $\lambda/4$ segment (from the bias injection points till the open end) presents an impedance converter, which translates an infinite open end impedance into essentially zero impedance between the dc coupling points. The effective microwave short zeroes the residual voltage and dramatically reduces radiation losses.

Another dissipation channel appears if the resonator mode couples to some parasitic resonance supported by the ground plane or the enclosure. For a fixed-frequency resonator, the odds that the resonance frequency will match some parasitic resonance are relatively low, and, if such an unlikely collision does take place, the problem could be eliminated by a few extra wire bonds across the chip that will shift the parasitic resonance in frequency. For tunable resonators, this simple solution obviously does not apply: all ground plane resonances present within the full tuning range (100–200 MHz for the presented design) should be either eliminated or decoupled from the resonator. In the presented resonators this challenge is conjointly addressed by a set of design solutions listed below. Firstly, the tuning fork geometry ensures that the microwave mode is localized in between the prongs. Secondly, the fractalized prong-to-prong capacitor provides per-unit-length capacitance much higher than that of a regular coplanar line; this translates into a very slow phase propagation velocity (approximately 4% of the speed of light) and a short resonator length of about 1.5 mm for a resonance frequency of 6 GHz. The transverse dimension is also rather compact: the prong-to-prong distance is 34 μm only. As the coupling to environmental resonances is proportional to the square of the dipole moment, our resonators are much more resilient to parasitics than the regular coplanar lines. Finally, elimination of dedicated dc lines and the simplest ground plane topology minimizes the spectral density of parasitics. In practice, we achieve above 75% yield: out of four resonances on a chip no more than one typically suffers from collision with parasitics within the full tuning range.

The resonators described here are fabricated from a 140 nm NbN film deposited on a 2-in. sapphire substrate. The desired structure is patterned with electron beam lithography and etched in a Ar : Cl_2 reactive ion plasma. The fabrication procedure is broadly similar to Ref. [32], where the Ar : Cl_2 reactive ion etching was used to ensure sharp sidewalls and to prevent lateral under-resist etching [34]. Au bonding pads are patterned and deposited in the next fabrication layer. Finally, with one extra exposure, the resonator (but not the ground) is thinned to the desired thickness (50 nm) using the same Ar : Cl_2 reactive ion etch process. This thickness yields a sheet kinetic inductance of approximately 4 pH/$\square$, which places the resonance frequency in the 4–8 GHz band. The ground plane thickness is left unchanged with sheet kinetic inductance approximately 1 pH/$\square$. This ensures that the typical frequencies of the ground plane resonances are placed above 8 GHz. Each 2-in. wafer yields 12 chips of size 10×9 mm^2. The chips with the capacitively coupled design has four resonators on the chip, while for the inductively coupled design, there is only a single resonator per chip.

Based on the normal state sheet resistance of the film, the kinetic inductance can be estimated as $L_k = \hbar R_N / \pi \Delta_0$, where $\hbar$ is the reduced Planck constant, R_N is the sheet resistance, and Δ_0 is the superconducting energy gap at 0 K. This corresponds to a kinetic inductance of 4 pH/$\square$ for the 50 nm thick film. This formula is approximate, but allows an estimation of L_k that can be used to model the resonator design with Sonnet's electromagnetic simulation software [35]. From the simulation, the position of the voltage node in the $3\lambda/4$ mode is obtained in order to connect the dc current leads at the optimal place.

III. RESULTS AND DISCUSSION

The fabricated devices are initially characterised in a 2 K liquid-helium cryostat. A vector network analyser is used to record the forward transmission (S_{21}) of the device; the measured S_{21} data are shown in Figs. 2(a) and 2(c). The resonance frequency smoothly changes as a function of the bias current following a parabolic dependence [cf. Figs. 2(b) and 2(d)] $L_k(I) \approx L_k(0)[1 + (I_{dc}/I_*)^2]$, where $L_k(0)$ is the kinetic inductance at zero current, I_{dc} is the bias current, and I_* is the nonlinearity parameter. The I_* extracted from a parabolic fit to Figs. 2(b) and 2(d) gives $I_* \approx 55$ mA such that $I_*/I_c \approx 5$, where I_c is the critical current of the resonator. These parameters can to some extent be tuned by varying the NbN film deposition conditions, such as the substrate temperature, N_2 partial pressure, and the flow rate.

For further characterization, we use a single-shot ^{3}He cryostat with a base temperature of 0.3 K. We record S_{21} scans at different temperatures, microwave excitation power levels, and dc tuning currents. From the recorded S_{21} scans, the internal and coupling quality factors are
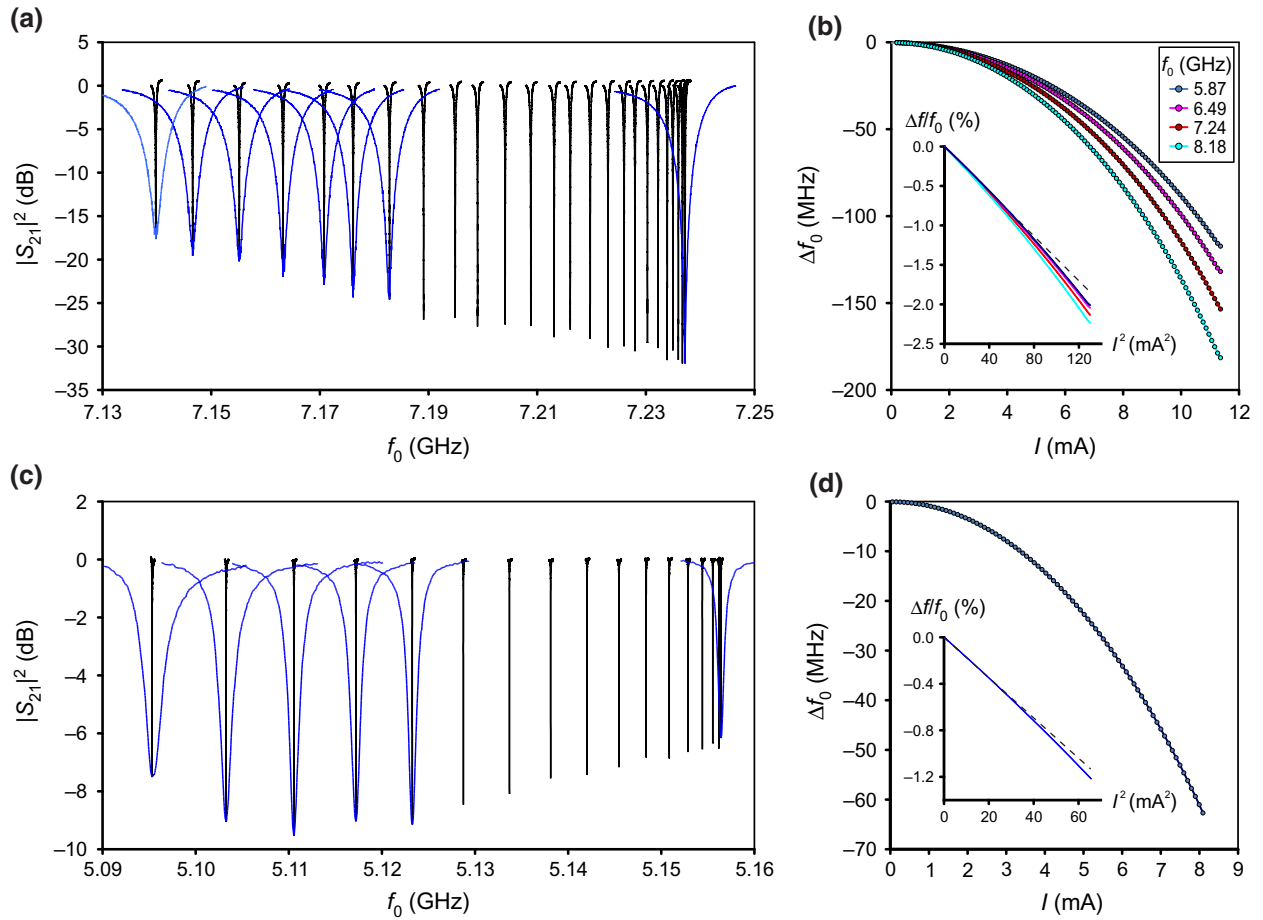
FIG. 2.   Frequency tuning with dc bias current. (a),(c) A set of S_{21} transmission resonances taken at different bias currents. The measured curves are shown in black; some curves (shown in blue) have been stretched in frequency [25 times for (a) and 100 times for (c)] to demonstrate the shape of the resonances. (b),(d) Frequency shift versus the bias current. Plots (a),(b) are for capacitively coupled and (c),(d) for inductively coupled designs. The data points are extracted from a set of S_{21} resonances taken with a current bias step of 0.1 mA. Insets present the same data as a function of I_{dc}^2 to illustrate the quadratic dependence of the frequency shift at low bias currents $\Delta f_0/f_0 = -1/2(I_{dc}/I_*)^2$ [30]. The dashed lines have slopes corresponding to $I_* = 59.5$ mA (b) and 54 mA (d).

extracted by fitting the data to the model provided in Ref. [36]; the aggregated results are shown in Fig. 3.

In Fig. 3(a) we present the internal quality factor as a function of dc tuning for different excitation powers for the measurements taken at 0.3 K. At zero tuning, Q_{int} depends on the excitation power (the power dependence is addressed later). Tuning the resonator frequency induces some excessive dissipation and Q_{int} decreases. Once Q_{int} approaches approximately 10^5, the tuning-related part of dissipation starts to dominate and the total Q factor does not depend on the excitation power anymore. Similar measurements are also performed at 0.7, 1.1, and 1.5 K. Quantifying the tuning-related quality factor as $1/Q_{\Delta f} = 1/Q_{int}(I) - 1/Q_{int}(0)$, we compose a plot shown in Fig. 3(b), where $1/Q_{\Delta f}$ is presented as a function of Δf_0^2. The fact that $1/Q_{\Delta f}$ does not depend on the excitation power or on the original (nontuned) Q_{int} clearly indicates that tuning-related dissipation is of a purely radiative nature. In

fact, the quadratic dependence on frequency tuning Δf_0 is what should be expected for radiative losses in our design: the dc current only affects the inductance of the $\lambda/2$ part of the resonator at the closed end [see Figs. 1(a) and 1(b)] and does not affect the inductance of the $\lambda/4$ part at the open end. As a result, as the resonance frequency is tuned, the position of the voltage nodes is slightly shifted away from the dc terminal coupling points. The voltage node shift is proportional to Δf_0, and thus the excessive radiation to Δf_0^2. For applications that do not require an extreme tuning time as short as $1/f_0$, the residual radiation losses can be further suppressed by replacing direct prong-to-ground links with simple low-pass filters.

An interesting feature of Fig. 3 is the ripple pattern that appears in the Q_{int} plots at near single-photon excitation powers and low temperatures. These ripples are reproducible on short (second to minute) timescales and nonreproducible on longer timescales (a couple of hours).
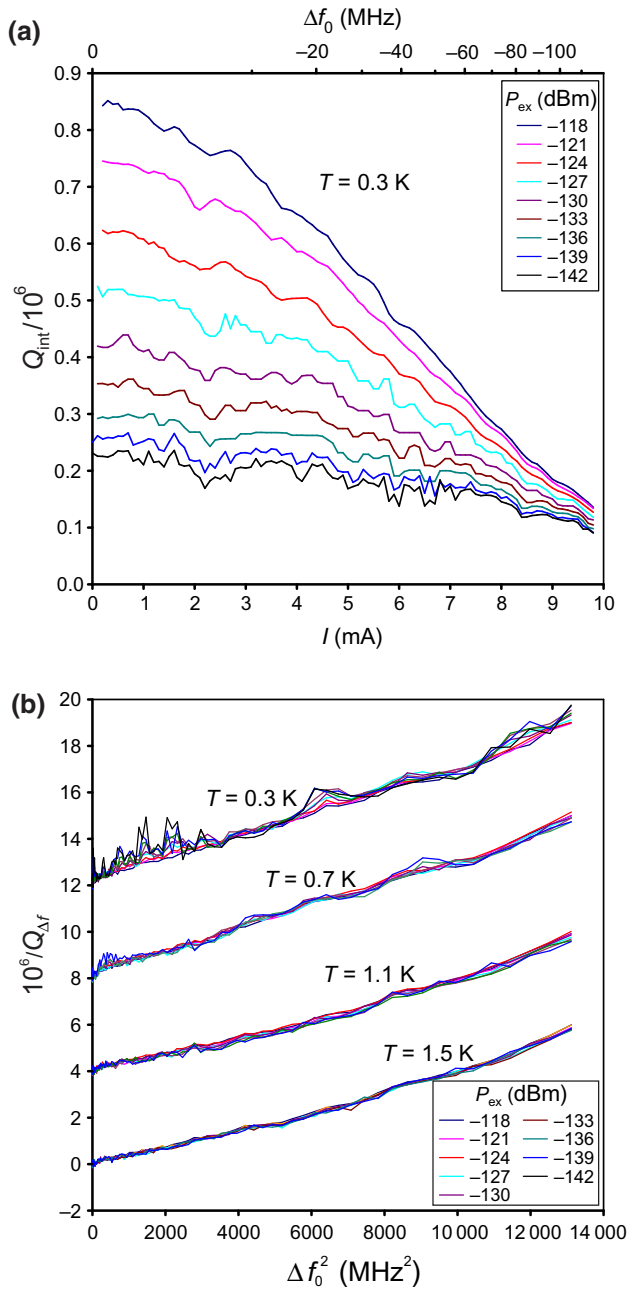
FIG. 3. Q factor versus frequency tuning. (a) As measured. (b) Tuning-related dissipation part $1/Q_{\Delta f}$. The plots are presented versus a square of the frequency shift Δf to illustrate the linear in $(\Delta f_0)^2$ dependence. The plots taken at different temperatures are offset for clarity (same offset for all excitation powers P_{ex}).

We attribute these fluctuations in Q_{int} to the interaction with an ensemble of charged two-level systems (TLSs), as previously reported in Ref. [37]. At high temperature or high excitation powers, the TLSs are saturated and the observed ripples are smeared. Also, as the energies of individual fluctuators are slowly varying in time [12], the ripple pattern is not reproducible on a longer time scale.
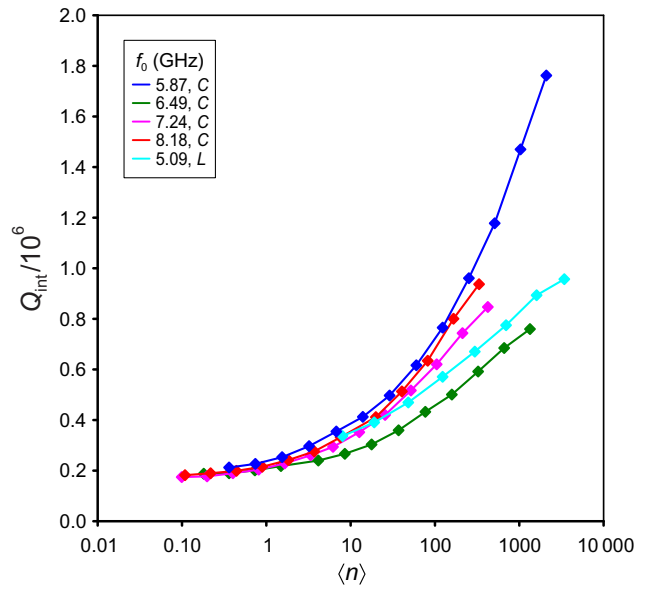

FIG. 4.   Internal Q factor for different photon occupations $\langle n \rangle$. In the legend C and L stand for capacitively and inductively coupled resonators. Measured at 0.3 K.

In Fig. 4 we present the power dependence of Q_{int} for all fiveresonators at 0.3 K. At near single-photon occupation numbers where TLS losses dominate the total dissipation, Q_{int} is similar for all the devices measured. For high photon occupation numbers, Q_{int} is limited by radiation losses, which varies from device to device by a factor of approximately 3. We attribute this inconsistency to different residual couplings to parasitics, deviations from left-right symmetry in the prongs of the tuning fork due to fabrication tolerances, etc.

To determine the tuning speed of the resonator, we follow the same methodology as in Ref. [21]. In Fig. 5 we present the tuning rate characterization measurements. The resonator is first excited at its unbiased resonance frequency $f_0 = 6.15$ GHz. Then a rectangular current tuning pulse is applied to detune the resonator to $f_0 - \delta f$. With a homodyne detection scheme, we measure the output microwave power as a function of time, presented in Fig. 5(b). Immediately after the frequency shift, the output signal is a sum of the excitation power at frequency f_0 and the power radiated by the resonator at $f_0 - \delta f$; the latter decays on a timescale $\tau = Q/\pi f_0$, during which we observe beatings [Fig. 5(b)] in the measured transmitted power. These beatings have a period precisely equal to $1/\delta f$. By extracting this period we can infer the instantaneous frequency at very short timescales. In Fig. 5(c) we track these beatings down to less than or approximately equal to 20 ns, thus demonstrating an almost instantaneous detuning of 40 MHz, i.e., in a time more than 1000 times shorter than the photon lifetime. We would like to stress that the instantaneous frequency shift of 40 MHz
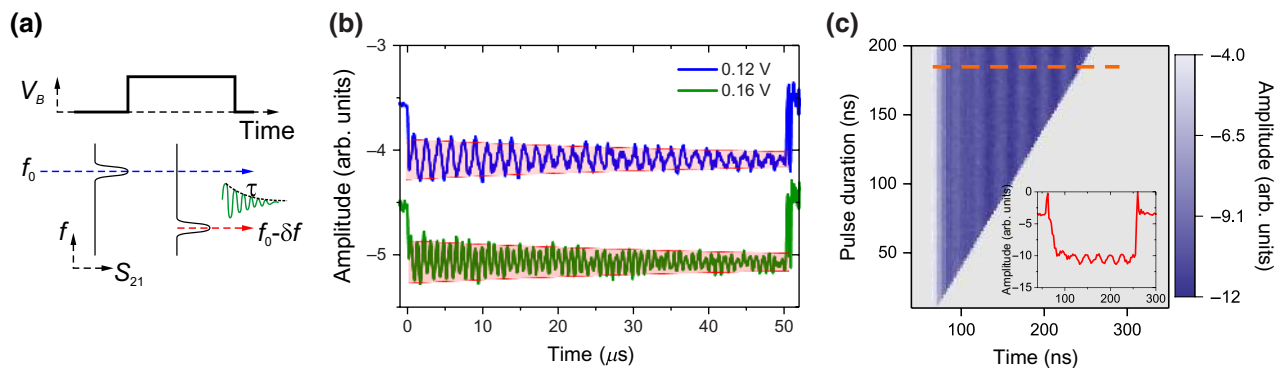
FIG. 5.　Characterization of the tuning response time. (a) Bias control pulse V_B (top) and dynamic resonator response. (b) Example of the measured homodyne detector output response to two detuning pulses (offset for clarity). The base resonator frequency is 6.15 GHz; the blue plot is for 0.6 MHz and the green plot is for 1.2 MHz detuning. The exponential energy decay with characteristic time $\tau = Q/\pi f_0 = 50\ \mu s$ is indicated by the envelopes. (c) Resonator response to detuning pulses of the same amplitude (corresponding to 40 MHz detuning) but different durations. Inset: cross section of the main color plot indicated with the dashed line.

could not be detected in a time shorter than approximately 1/40 MHz = 25 ns, i.e., the reported 20 ns time is actually limited by the resolution of the readout method itself, rather than the internal device response time, which is expected to be even faster.

We have previously demonstrated that field resilient fractal resonators can be used as a core of on-chip ESR spectrometers [14,15]. Compared to a standard ESR bulk cavity design, the microwave field volume in a planar resonator is squeezed up to 10^6 times, resulting in a greatly enhanced spin-to-microwave coupling. In combination with a high Q factor provided by superconducting resonators, this translates to exceptional ESR sensitivity, with a minimum detectable number of spins of a few hundred [38,39]. The microwave field in a planar resonator is naturally localized around the substrate surface, which provides selective sensitivity to surface spins and deposited nanoscale clusters [14,32]. Magnetic field resilience is instrumental for ESR applications, which generally present a challenge for superconducting designs. To achieve high-field resilience, we reapply the design ideas previously exploited in Ref. [32]. Specifically, we implement the fractalized ground plane design to eliminate the magnetic flux focusing. The ground plane in both *C*- and *L*-coupled designs is split in such a way that a flux escape path is available for all open (no film) areas, and superconducting loops are thus avoided. Finally (and most importantly), the narrow thin film elements composing a fractal structure effectively expel vortices. Taking all these precautions, we demonstrate that tunable resonators can be made equally suitable for surface spin detection. In Fig. 6, we present an ESR spectrum [i.e., magnetic-field-dependent dissipation part $1/Q_B = 1/Q_{int}(B) - 1/Q_{int}(0)$] obtained with the tunable resonator by scanning the magnetic field up to 500 mT.

The spectrum reveals the spins present in the bulk and on the surface of the sapphire substrate [14]. From our

previous studies we know the number of spins constituting the main ESR peak centered at 180 mT [32]. As the area under the peak scales roughly in proportion with the number of constituent spins, the number of spins contributing to a peak positioned at 235 mT (see the inset of Fig. 6) is estimated to be 10^3–10^4. Remarkably, even for such a small number of spins, the signal-to-noise ratio in the inset of Fig. 6 is still quite decent. The frequency tuning option provides an ESR spectrometer with an additional functionality: by varying the probe frequency by Δf_0 and measuring the corresponding resonance peak shift ΔB one can directly assess an equivalent g factor $g = h\Delta f_0/(\mu_B \Delta B) = 2.4$ for the peak in the inset of Fig. 6.

Finally, we note that the dc bias current generates a magnetic field that could be non-negligible for some applications. A simple estimation shows that the 10 mA current creates a field of 3 mT circulating around the prong. As this field is orthogonal to the external field $B_{ext} = 230$ mT, the total field is only incremented by 0.02 mT. This is an order of magnitude below the resonance linewidth in Fig. 6 and therefore not an issue in our case. However, it may need to be accounted for when coupling to qubits or measuring spin systems with exceptionally sharp ESR resonances.

IV. DETAILS OF THE MEASUREMENT SETUP

The measurements at 0.3 K (Figs. 2–4 and 6) are performed in a single-shot liquid ^{3}He refrigerator. The rf excitation channel is attenuated by 80 dB for thermalization, the readout is performed through the isolator mounted at the 3 K stage, followed by a cryogenic amplifier with 2 K noise temperature. The dc wiring, thermalized to all intermediate stages, has a resistance of 10 Ω for low-pass filtering.

The fast tuning measurements (Fig. 5) are performed in a dilution refrigerator with a base temperature of 10 mK. For dynamic experiments, proper filtering of the tuning current
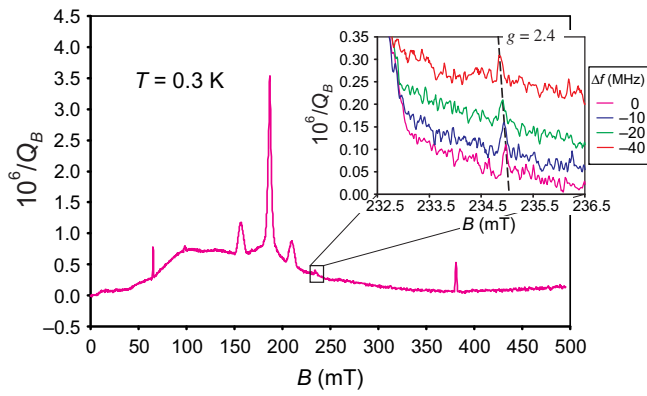
FIG. 6. Tunable resonator as a core of the ESR spectrometer. Main plot: ESR spectrum (excessive dissipation as a function of the magnetic field) taken with a resonator operating at a base resonance frequency. The spectrum reveals paramagnetic impurities in the sapphire substrate and the spins of surface absorbants. Inset: a set of ESR spectra taken with different frequency shifts as indicated in the legend. The slope of the dashed line corresponds to a g factor of 2.4. Data taken with a resonator with base frequency $f_0 = 5.157$ GHz [Fig. 2(c)]. All spectra taken with a microwave power of 70 pW circulating in the resonator (approximately 500 photons). The total measurement time for a single spectrum is one hour.

lines is important as the bias circuitry should admit both a wide bandwidth and high currents. A low-loss coaxial line is used with 0 dB attenuators at all temperature stages of the dilution refrigerator, and 250 MHz low-pass filters are used at 10 mK. The return dc current is directed through a similar line to a 50 Ω termination mounted on the 800 mK stage. The tuning pulses are generated by an arbitrary waveform voltage source in series with a 100 Ω resistor. The rf readout is done through the input line with a total attenuation of 75 dB and on the output channel two cold isolators are installed in series prior to a low noise cryogenic HEMT amplifier.

V. SUMMARY

In summary, we present a superconducting microwave resonator design that allows for frequency tuning without substantial compromise of the resonator quality factor. We demonstrate that the internal Q factor holds the value above 10^5 down to the single-photon limit over the entire tuning range up to 200 MHz. The dominant loss mechanism is residual radiation through the current bias control lines that could be further suppressed with low-pass filters. We demonstrate that a full-scale frequency shift can be performed in a time shorter than a 10^{-3} fraction of the photon lifetime.

The quasifractal resonator design allows for operation in high magnetic fields. Here we demonstrate magnetic field resilience up to 0.5 T. We argue that, by shrinking the minimum features in the design down to approximately 100 nm

or by introducing high-density perforation of the superconducting film, the resonators can be made operational in magnetic fields above 5 T, as previously demonstrated in Refs. [40] and [41].

When the resonator is used for ESR spectrometry, the frequency tuning allows for determination of the effective g factor of the spins. Owing to a high quality factor of our resonators, the g factor can be reliably measured on spin ensembles as small as approximately 1000 spins, which is close to state of the art in the field [39]. In perspective, frequency tunable resonators pave the way for the implementation of advanced ESR techniques with on-chip devices, such as pulsed ESR and electron-electron double resonance detected NMR [42]. Last, but not least, we foresee many potential applications for fast tunable high-Q resonators in the rapidly progressing field of quantum computing.

[1] M. D. Reed, B. R. Johnson, A. A. Houck, L. DiCarlo, J. M. Chow, D. I. Schuster, L. Frunzio, and R. J. Schoelkopf, Fast reset and suppressing spontaneous emission of a superconducting qubit, Appl. Phys. Lett. **96**, 203110 (2010).

[2] M. Simoen, C. Chang, P. Krantz, J. Bylander, W. Wustmann, V. Shumeiko, P. Delsing, and C. Wilson, Characterization of a multimode coplanar waveguide parametric amplifier, J. Appl. Phys. **118**, 154501 (2015).

[3] W. Wustmann and V. Shumeiko, Parametric resonance in tunable superconducting cavities, Phys. Rev. B **87**, 184501 (2013).

[4] P. K. Day, H. G. LeDuc, B. A. Mazin, A. Vayonakis, and J. Zmuidzinas, A broadband superconducting detector suitable for use in large arrays, Nature **425**, 817 (2003).

[5] S. De Graaf, A. Danilov, and S. Kubatkin, Coherent interaction with two-level fluctuators using near field scanning microwave microscopy, Sci. Rep. **5**, 17176 (2015).

[6] S. E. de Graaf, A. Danilov, A. Adamyan, and S. Kubatkin, A near-field scanning microwave microscope based on a superconducting resonator for low power measurements, Rev. Sci. Instrum. **84**, 023706 (2013).

[7] S. Geaney, D. Cox, T. Hönigl-Decrinis, R. Shaikhaidarov, S. Kubatkin, T. Lindström, A. Danilov, and S. de Graaf, Near-field scanning microwave microscopy in the single photon regime, Sci. Rep. **9**, 12539 (2019).

[8] M. Pierre, I.-M. Svensson, S. Raman Sathyamoorthy, G. Johansson, and P. Delsing, Storage and on-demand release

of microwaves using superconducting resonators with tunable coupling, Appl. Phys. Lett. **104,** 232604 (2014).

[9] I.-C. Hoi, C. Wilson, G. Johansson, T. Palomaki, B. Peropadre, and P. Delsing, Demonstration of a Single-Photon Router in the Microwave Regime, Phys. Rev. Lett. **107,** 073601 (2011).

[10] Y. Yin, Y. Chen, D. Sank, P. O'Malley, T. White, R. Barends, J. Kelly, E. Lucero, M. Mariantoni, A. Megrant, C. Neill, A. Vainsencher, J. Wenner, A. Korotkov, A. Cleland, and J. Martinis, Catch and Release of Microwave Photon States, Phys. Rev. Lett. **110,** 107001 (2013).

[11] G. Wendin, Quantum information processing with superconducting circuits: A review, Rep. Prog. Phys. **80,** 106001 (2017).

[12] C. Müller, J. H. Cole, and J. Lisenfeld, Towards understanding two-level-systems in amorphous solids: Insights from quantum circuits, Rep. Prog. Phys. **82,** 124501 (2019).

[13] E. Paladino, Y. Galperin, G. Falci, and B. Altshuler, 1/f noise: Implications for solid-state quantum information, Rev. Mod. Phys. **86,** 361 (2014).

[14] S. de Graaf, A. Adamyan, T. Lindström, D. Erts, S. Kubatkin, A. Y. Tzalenchuk, and A. Danilov, Direct Identification of Dilute Surface Spins on Al_2O_3: Origin of Flux Noise in Quantum Circuits, Phys. Rev. Lett. **118,** 057703 (2017).

[15] S. De Graaf, L. Faoro, J. Burnett, A. Adamyan, A. Y. Tzalenchuk, S. Kubatkin, T. Lindström, and A. Danilov, Suppression of low-frequency charge noise in superconducting resonators by surface spin desorption, Nat. Commun. **9,** 1143 (2018).

[16] Z. Kim, C. Vlahacos, J. Hoffman, J. Grover, K. Voigt, B. Cooper, C. Ballard, B. Palmer, M. Hafezi, J. Taylor, *et al.*, Thin-film superconducting resonator tunable to the ground-state hyperfine splitting of ^{87}Rb, AIP Adv. **1,** 042107 (2011).

[17] J. Healey, T. Lindström, M. Colclough, C. Muirhead, and A. Y. Tzalenchuk, Magnetic field tuning of coplanar waveguide resonators, Appl. Phys. Lett. **93,** 043513 (2008).

[18] S. Chaudhuri, D. Li, K. Irwin, C. Bockstiegel, J. Hubmayr, J. Ullom, M. Vissers, and J. Gao, Broadband parametric amplifiers based on nonlinear kinetic inductance artificial transmission lines, Appl. Phys. Lett. **110,** 152601 (2017).

[19] B. H. Eom, P. K. Day, H. G. LeDuc, and J. Zmuidzinas, A wideband, low-noise superconducting amplifier with high dynamic range, Nat. Phys. **8,** 623 (2012).

[20] R. P. Erickson, M. R. Vissers, M. Sandberg, S. R. Jefferts, and D. P. Pappas, Frequency Comb Generation in Superconducting Resonators, Phys. Rev. Lett. **113,** 187002 (2014).

[21] M. Sandberg, C. Wilson, F. Persson, T. Bauch, G. Johansson, V. Shumeiko, T. Duty, and P. Delsing, Tuning the field in a microwave resonator faster than the photon lifetime, Appl. Phys. Lett. **92,** 203501 (2008).

[22] Z. Wang, Y. Zhong, L. He, H. Wang, J. M. Martinis, A. Cleland, and Q. Xie, Quantum state characterization of a fast tunable superconducting resonator, Appl. Phys. Lett. **102,** 163503 (2013).

[23] O. Kennedy, J. Burnett, J. Fenton, N. Constantino, P. Warburton, J. Morton, and E. Dupont-Ferrier, Tunable Nb Superconducting Resonator Based on a Constriction Nano-Squid Fabricated with a Ne Focused Ion Beam, Phys. Rev. Appl. **11,** 014006 (2019).

[24] K. Osborn, J. Strong, A. J. Sirois, and R. W. Simmonds, Frequency-tunable Josephson junction resonator for quantum computing, IEEE Trans. Appl. Supercond. **17,** 166 (2007).

[25] A. Palacios-Laloy, F. Nguyen, F. Mallet, P. Bertet, D. Vion, and D. Esteve, Tunable resonators for quantum circuits, J. Low Temp. Phys. **151,** 1034 (2008).

[26] I.-M. Svensson, M. Pierre, M. Simoen, W. Wustmann, P. Krantz, A. Bengtsson, G. Johansson, J. Bylander, V. Shumeiko, and P. Delsing, in *Journal of Physics: Conference Series* (IOP Publishing, 2018), Vol. 969, p. 012146.

[27] A. Megrant, C. Neill, R. Barends, B. Chiaro, Y. Chen, L. Feigl, J. Kelly, E. Lucero, M. Mariantoni, P. J. O'Malley, *et al.*, Planar superconducting resonators with internal quality factors above one million, Appl. Phys. Lett. **100,** 113510 (2012).

[28] S. J. Bosman, V. Singh, A. Bruno, and G. A. Steele, Broadband architecture for galvanically accessible superconducting microwave resonators, Appl. Phys. Lett. **107,** 192602 (2015).

[29] A. Adamyan, S. Kubatkin, and A. Danilov, Tunable superconducting microstrip resonators, Appl. Phys. Lett. **108,** 172601 (2016).

[30] M. R. Vissers, J. Hubmayr, M. Sandberg, S. Chaudhuri, C. Bockstiegel, and J. Gao, Frequency-tunable superconducting resonators via nonlinear kinetic inductance, Appl. Phys. Lett. **107,** 062601 (2015).

[31] A. Asfaw, A. Sigillito, A. Tyryshkin, T. Schenkel, and S. Lyon, Multi-frequency spin manipulation using rapidly tunable superconducting coplanar waveguide microresonators, Appl. Phys. Lett. **111,** 032601 (2017).

[32] S. de Graaf, A. Danilov, A. Adamyan, T. Bauch, and S. Kubatkin, Magnetic field resilient superconducting fractal resonators for coupling to free spins, J. Appl. Phys. **112,** 123905 (2012).

[33] S. E. de Graaf, D. Davidovikj, A. Adamyan, S. Kubatkin, and A. Danilov, Galvanically split superconducting microwave resonators for introducing internal voltage bias, Appl. Phys. Lett. **104,** 052601 (2014).

[34] D. Niepce, Licenciate thesis, Chalmers University of Technology, 2018.

[35] Sonnet Electromagnetic Simulation Software. http://www.sonnetsoftware.com/products/sonnet-suites/, 2019.

[36] S. Probst, F. Song, P. Bushev, A. Ustinov, and M. Weides, Efficient and robust analysis of complex scattering data under noise in microwave resonators, Rev. Sci. Instrum. **86,** 024706 (2015).

[37] J. D. Brehm, A. Bilmes, G. Weiss, A. V. Ustinov, and J. Lisenfeld, Transmission-line resonators for the study of individual two-level tunneling systems, Appl. Phys. Lett. **111,** 112601 (2017).

[38] S. Probst, A. Bienfait, P. Campagne-Ibarcq, J. Pla, B. Albanese, J. Da Silva Barbosa, T. Schenkel, D. Vion, D. Esteve, K. Mølmer, *et al.*, Inductive-detection

electron-spin resonance spectroscopy with 65 spins/Hz sensitivity, Appl. Phys. Lett. **111,** 202604 (2017).

[39] V. Ranjan, S. Probst, B. Albanese, T. Schenkel, D. Vion, D. Esteve, J. Morton, and P. Bertet, Electron spin resonance spectroscopy with femtoliter detection volume, arXiv:2002.03669, 2020.

[40] J. Kroll, F. Borsoi, K. van der Enden, W. Uilhoorn, D. de Jong, M. Quintero-Pérez, D. van Woerkom, A. Bruno, S. Plissard, D. Car, *et al.*, Magnetic-Field-Resilient Superconducting Coplanar-Waveguide Resonators for Hybrid Circuit Quantum Electrodynamics Experiments, Phys. Rev. Appl. **11,** 064053 (2019).

[41] N. Samkharadze, A. Bruno, P. Scarlino, G. Zheng, D. P. DiVincenzo, L. DiCarlo, and L. Vandersypen, High-Kinetic-Inductance Superconducting Nanowire Resonators for Circuit QED in a Magnetic Field, Phys. Rev. Appl. **5,** 044004 (2016).

[42] N. Cox, A. Nalepa, W. Lubitz, and A. Savitsky, Eldor-detected NMR: A general and robust method for electron-nuclear hyperfine spectroscopy? J. Magnet. Res. **280,** 63 (2017).